ELSEVIER

Journal of Organometallic Chemistry 580 (1999) 225–233

Journal of Organometallic Chemistry

Site-selective carbonyl substitution in the mixed-metal cluster anion $[H_2Ru_3Ir(CO)_{12}]^-$: synthesis and characterization of phosphine, phosphite, arsine and stibine derivatives

Georg Süss-Fink *, Susanne Haak, Vincent Ferrand, Antonia Neels, Helen Stoeckli-Evans

Institut de Chimie, Université de Neuchâtel, avenue de Bellevaux 51, CH-2000 Neuchâtel, Switzerland

Received 21 September 1998

Abstract

The reaction of the mixed-metal carbonyl cluster anion $[H_2Ru_3Ir(CO)_{12}]^-$ with PPh_3, PMe_3, $P(OPh)_3$, $AsPh_3$ or $SbPh_3$ leads to the mono-substituted derivatives $[H_2Ru_3Ir(CO)_{11}L]^-$ (L = PPh_3 **1**, L = PMe_3 **2**, L = $P(OPh)_3$ **3**, L = $AsPh_3$ **4**, L = $SbPh_3$ **5**). Protonation of the anions **1**–**5** gives the neutral trihydrido derivatives $H_3Ru_3Ir(CO)_{11}L$ (L = PPh_3 **6**, L = PMe_3 **7**, L = $P(OPh)_3$ **8**, L = $AsPh_3$ **9**, L = $SbPh_3$ **10**). All new tetranuclear clusters invariably show a tetrahedral arrangement of the Ru_3Ir skeleton, as predicted for 60 e systems. The ligand L is coordinated to one of the ruthenium atoms, except in the case of L = PMe_3 where two substitution isomers are observed. While the anionic isomers $[H_2Ru_3Ir(CO)_{11}(PMe_3)]^-$ (**2**) could not be separated, the corresponding neutral isomers $H_3Ru_3Ir(CO)_{11}(PMe_3)$ (**7**) could be resolved by thin-layer chromatography. In isomer **7a**, the phosphine ligand is coordinated to one of the ruthenium atoms, whereas in isomer **7b** the PMe_3 ligand is bonded to the iridium atom. The molecular structures of **1**, **7b**, **8** and **9** were confirmed by a single-crystal X-ray structure analysis.

Keywords: Mixed-metal clusters; Ruthenium; Iridium; Carbonyls; Hydrido; Phosphine

1. Introduction

The last three decades have witnessed a steadily growing interest in mixed-metal cluster chemistry due to the inherent catalytic potential of mixed-metal complexes [1]. The combination of different metals in the same complex can give rise to an enhanced catalytic activity because of the direct interaction of different metal atoms as well as of the interaction of the substrate with different metal centers [2].

We recently reported a series of Ru_3Ir mixed-metal clusters [3] which showed a high catalytic activity for the carbonylation of methanol [4]. In this context, the substitution of carbonyls by other ligands is interesting with respect to the catalytic properties. Most of the known d^8–d^9 tetranuclear mixed-metal clusters containing PR_3 ligands are neutral, e.g. $HRu_3Ir(CO)_{12}(PPh_3)$, $H_3Ru_3Ir(CO)_{11}(PPh_3)$ [5], $H_{2-x}Ru_{4-x}Ir_x(CO)_{12}(PPh_3)$ ($x = 0$ or 1) [6], $Ru_3Rh_2(\mu_4\text{-PPh})(CO)_{13}(PEt_3)$ [7], $HRu_3Rh_2(CO)_{13}(PPh_3)(AuPPh_3)$ [8], $HRuRh_3(CO)_{10}(PPh_3)_2$ [9], $HRuCo_3(CO)_{11}(PPh_3)$ [10], $HRuRh_3(CO)_{11}(PMe_3)$, $HRuCo_3(CO)_{11}(PMe_3)$ or $HRuCo_2Rh(CO)_{11}(PMe_2Ph)$ [11]. Only few anionic examples are published in the literature: Thus, the cluster anion $[Ru_3Rh(CO)_{13}]^-$ reacts with PPh_3 to give the substituted derivative $[Ru_3Rh(CO)_{12}(PPh_3)]^-$ [12], whereas the reaction of the hydrogenated derivative $[H_2Ru_3Rh(CO)_{12}]^-$ with PPh_3 under the same conditions leads to a mixture of the neutral clusters $H_2Ru_3Rh_2(CO)_{13}(PPh_3)$ and $H_2Ru_3Rh_2(CO)_{12}(PPh_3)_2$ [13]; the expected phosphine derivative $[H_2Ru_3Rh(CO)_{11}(PPh_3)]^-$ was obtained by treating $H_2Ru_3Rh(CO)_{10}(PPh_3)(\mu\text{-COMe})$ with a $K[BHBu^s_3]$–THF solution [14].

* Corresponding author. Tel.: +41-32-7182405; fax: +41-32-7182511.

E-mail address: suess-fink@ich.unine.ch (G. Süss-Fink)

0022-328X/99/$ - see front matter
PII: S0022-328X(98)01151-6

In this paper we report the synthesis and characterization of a series of mono-substituted tetranuclear cluster anions $[H_2Ru_3Ir(CO)_{11}L]^-$ as well as their protonated derivatives $H_3Ru_3Ir(CO)_{11}L$ ($L = PPh_3$, PMe_3, $P(OPh)_3$, $AsPh_3$, $SbPh_3$).

2. Results and discussion

2.1. Synthesis and characterization of the derivatives $[H_2Ru_3Ir(CO)_{11}L]^-$ ($L = PPh_3$, PMe_3, $P(OPh)_3$, $AsPh_3$ and $SbPh_3$)

The thermal reaction between the dihydrido anion $[H_2Ru_3Ir(CO)_{12}]^-$ [3] and equimolar quantities of PPh_3, $P(OPh)_3$, $AsPh_3$ or $SbPh_3$ in tetrahydrofuran (THF) affords the mono-substituted derivatives $[H_2Ru_3Ir(CO)_{11}(PPh_3)]^-$ (**1**), $[H_2Ru_3Ir(CO)_{11}(PMe_3)]^-$ (**2**), $[H_2Ru_3Ir(CO)_{11}\{P(OPh)_3\}]^-$ (**3**), $[H_2Ru_3Ir(CO)_{11}(AsPh_3)]^-$ (**4**) and $[H_2Ru_3Ir(CO)_{11}(SbPh_3)]^-$ (**5**), which can be isolated as the bis(triphenylphosphoranylidene)ammonium salts from a mixture of either CH_2Cl_2/ether/hexane or ethanol/pentane (Eq. (1)).

$$[H_2Ru_3Ir(CO)_{12}]^- + L \longrightarrow [H_2Ru_3Ir(CO)_{11}L]^- + CO \quad (1)$$

L	PPh_3	PMe_3	$P(OPh)_3$	$AsPh_3$	$SbPh_3$
	1	2	3	4	5

The compounds **1**, **3**, **4** and **5** show an almost identical ν(CO) pattern in the infrared spectrum (six absorptions of terminal carbonyl ligands and three bands in the region of carbonyl bridges), indicating the same type of structure and the same ligand envelope for the four clusters (Table 1).

The room-temperature ^{1}H-NMR spectra show one sharp signal for the two hydride ligands around δ −20 ppm. In compounds **1** and **3**, which contain a phosphorus ligand, the signal is split by the ^2J(P–H) coupling of 10.6 Hz (for **1**) and 10.5 Hz (for **3**). The signal centered at δ 7.48 ppm (multiplet) is attributed to the protons of the $[N(PPh_3)_2]^+$ cations. In the ^{31}P-NMR spectra of **1** and **3** two signals are observed, one at δ 21.7 ppm for the $[N(PPh_3)_2]^+$ cations, the second one for the phosphorus ligand. In each case the signal is shifted downfield in comparison with the free ligand and appears as a multiplet due to the coupling with the hydride ligands (Table 1).

All spectroscopic data suggest that **1**, **3**, **4** and **5** have the same ligand arrangement as found for the isoelectronic cluster anion $[H_2Ru_3Rh(CO)_{11}(PPh_3)]^-$ [14] where the PPh_3 ligand is coordinated to the apical ruthenium atom in the direct neighborhood of the hydride ligands. This hypothesis is confirmed by the molecular structure of the derivative $[H_2Ru_3Ir(CO)_{11}(PPh_3)]^-$ (**1**) (see Section 2.2).

In the case of PMe_3, the reaction leads to a mixture of three anionic clusters, two of which are presumably isomers of $[H_2Ru_3Ir(CO)_{11}(PMe_3)]^-$ (**2**), while the third species could be a disubstituted anion $[H_2Ru_3Ir(CO)_{10}(PMe_3)_2]^-$. The comparison of the ^{1}H-NMR spectrum (recorded at −60°C) of the mixture with the spectra of the anions **1**, **3**, **4** and **5** allows the assignment of the signals of the expected mono-substituted derivative $[H_2Ru_3Ir(CO)_{11}(PMe_3)]^-$ (**2a**), in which PMe_3 is coordinated to one of the ruthenium atoms [hydride signal at δ −20.60 ppm as a doublet with a ^2J(P–H) coupling constant of 12.9 Hz]. For the second isomer **2b**, a doublet at δ −19.86 ppm is observed in the hydride region of the ^{1}H-NMR spectrum, showing the coupling of the two equivalent hydrides with the phosphorus atom [^2J(P–H) = 5.0 Hz]. A doublet of doublets at δ −19.82 ppm [^2J(P–H) = 12.4 Hz, ^3J(P–H) = 2.9 Hz] is tentatively attributed to the disubstituted anion $[H_2Ru_3Ir(CO)_{10}(PMe_3)_2]^-$. While the ^{31}P-NMR signal of **2a** appears at δ −6.67 ppm, that of **2b** is found at δ −37.45 ppm (Table 1). The second isomer **2b** is considered as the cluster $[H_2Ru_3Ir(CO)_{11}(PMe_3)]^-$ in which the PMe_3 ligand is co-ordinated to the iridium atom. This hypothesis is strongly supported by the single-crystal X-ray structure analysis of $H_3Ru_3Ir(CO)_{11}(PMe_3)$ (**7b**), the protonation product of **2b** (see Section 2.3). For the disubstituted anion $[H_2Ru_3Ir(CO)_{10}(PMe_3)_2]^-$, present in the mixture, the ^{31}P-NMR spectrum shows two signals (doublets) at δ −8.97 ppm and δ −43.90 ppm [^2J(P–H) = 33.4 Hz].

2.2. Molecular structure of $[H_2Ru_3Ir(CO)_{11}(PPh_3)]^-$ **1**

The molecular structure of **1** was confirmed by a single-crystal X-ray structure analysis. Suitable crystals were grown by slow diffusion of hexane into an ether solution of the $[N(PPh_3)_2]^+$ salt of **1**. The crystal consists of discrete $[N(PPh_3)_2]^+$ cations and $[H_2Ru_3Ir(CO)_{11}(PPh_3)]^-$ anions, showing normal intermolecular contacts between the atoms of the ions. The structure of **1** is depicted in Fig. 1, and selected bonds and angles are given in Table 2.

The crystal structure of **1** comprises a distorted tetrahedron of the Ru_3Ir metal core because of the two bridging hydride ligands. The two hydrido-bridged Ru–Ru edges are significantly longer than the other metal–metal bonds, with 2.964(6) Å for Ru(1)–Ru(2) and the 2.960(6) Å for Ru(1)–Ru(3). The Ru(2)–Ru(3) bond as well as the Ru–Ir distances are in the range of 2.74–2.77 Å. The phosphine ligand is coordinated to the apical Ru atom which is also bonded to the hydride ligands, the Ru(1)–P(1) bond length being 2.342(2) Å. In the basal Ru_2Ir triangle each metal–metal bond is bridged by one CO group which lie almost in the Ru(2)–Ru(3)–Ir(1) plane; the tetrahedral angles being −4.24(13), −0.44(14) and −1.25(15)°. The arrange-

Table 1
Infrared, ^{1}H-NMR and ^{31}P-NMR spectroscopy data

Complex	IR ν_{CO} [cm^{-1}][a]	δ (^{1}H) [ppm][b]	δ (^{31}P) [ppm][c]
$[N(PPh_3)_2][H_2Ru_3Ir(CO)_{11}(PPh_3)]$ (anion **1**)	2041(m), 2007(vs), 1988(vs), 1953(s), 1939(m), 1931(m), 1852(w), 1801(m), 1788(s)	−19.94 [d, 2 H, H^-, ^2J(P–H) = 10.6 Hz] 7.29–7.66 {m, 45 H, $[N(PPh_3)_2]^+$ and PPh_3}	39.50 (s, PPh_3) 21.91 {s, $[N(PPh_3)_2]^+$}
$[N(PPh_3)_2][H_2Ru_3Ir(CO)_{11}(Pme_3)]$ (anions **2**)	2055(w), 2039(w), 2005(s), 1985(vs), 1963(m), 1951(m), 1932(m), 1917(sh), 1885(sh), 1841(vw), 1806(sh), 1788(m), 1776(m)	−20.60 [d, 2 H, H^-, ^2J(P–H) = 12.9 Hz] 1.32 [d, 9 H, PMe_3, ^2J(P–H) = 9.0 Hz] 7.39–7.70 {m, 30 H, $[N(PPh_3)_2]^+$} (**2a**) −19.86 [d,2 H, H^-, ^2J(P–H) = 5.0 Hz) 1.65 [d, 9 H, PMe_3, ^2J(P–H) = 10.5 Hz] 7.39–7.70 {m, 30 H, $[N(PPh_3)_2]^+$} (**2b**)	−6.67 (m, PMe_3) 21.75 {s, $[N(PPh_3)_2]^+$} (**2a**) −37.45 (m, PMe_3) 21.75 {s, $[N(PPh_3)_2]^+$} (**2b**)
$[N(PPh_3)_2]$ $[H_2Ru_3Ir(CO)_{11}\{P(OPh)_3\}]$ (anion **3**)	2049(m), 2020(s), 1991(vs), 1974(sh), 1961(m), 1939(m), 1859(w), 1794(s), 1785(sh)	−20.57 [d, 2 H, H^-, ^2J(P–H) = 10.6 Hz] 7.08–7.69 {m, 45 H, $[N(PPh_3)_2]^+$ and $P(OPh)_3$}	133.21 (m, $P(OPh)_3$) 21.79 {s, $[N(PPh_3)_2]^+$}
$[N(PPh_3)_2]$ $[H_2Ru_3Ir(CO)_{11}(AsPh_3)]$ (anion **4**)	2041(m), 2007(s), 1989(vs), 1952(m), 1941(m), 1933(m), 1852(w), 1802(m), 1790(m)	−19.94 (s, 2 H, H^-) 7.33–7.68 {m, 45 H, $[N(PPh_3)_2]^+$ and $AsPh_3$}	–[d]
$[N(PPh_3)_2]$ $[H_2Ru_3Ir(CO)_{11}(SbPh_3)]$ (anion **5**)	2042(m), 2006(vs), 1991(vs), 1953(m), 1942(m), 1934(sh), 1852(vw), 1804(m), 1790(m)	−20.21 (s, 2 H, H^-) 7.31–7.68 {m, 45 H, $[N(PPh_3)_2]^+$ and $SbPh_3$}	–[d]
$H_3Ru_3Ir(CO)_{11}(PPh_3)$ (**6**)	2095(w), 2070(s), 2050(vs), 2031(m), 2017(w), 2008(w), 1991(vw)	17.88 (t, 1 H, H^-) −16.94 [dd, 2 H, H^-, ^2J(P–H) = 11.2 Hz, ^2J(H–H) = 2.6 Hz] 7.38–7.44 (m, 15 H, PPh_3)	34.19 (m, PPh_3)
$H_3Ru_3Ir(CO)_{11}(PMe_3)$ (**7a**)	2095(w), 2069(s), 2048(vs), 2029(s), 2016(w), 2005(m), 1988(w), 1969(vw)	−18.10 [t, 1 H, H^-, ^2J(H–H) = 3.0 Hz] −17.80 [dd, 2 H, H^-, ^2J(P−H) = 13.4 Hz, ^2J(H–H) = 3.0 Hz] 1.68 [d, 9 H, PMe_3, ^2J(P–H) = 9.8 Hz]	−4.20 (m, PMe_3)
$H_3Ru_3Ir(CO)_{11}(PMe_3)$ (**7b**)	2093(w), 2068(vs), 2047(vs), 2029(s), 1999(m)	−17.79 [d, 2 H, H^-, ^2J(P–H) = 10.8 Hz] −16.75, −20.13, −20.17 (3 s, 1 H, H^-) 2.01 [d, 9 H, H^-, ^2J(P–H) = 10.3 Hz]	−46.65 (m, PMe_3)
$H_3Ru_3Ir(CO)_{11}\{P(OPh)_3\}$ (**8**)	2099(w), 2073(s), 2055(vs), 2037(s), 2021(w), 2011(w), 1998(sh)	−18.25 [t, 1 H, H^-, ^2J(H–H) = 2.5 Hz] −17.96 [dd, 2 H, H^-, ^2J(P–H) = 12.0 Hz, ^2J(H–H) = 2.5 Hz]	122.92 [t, $P(OPh)_3$, ^2J(P–H) = 10.5 Hz]
$H_3Ru_3Ir(CO)_{11}(AsPh_3)$ (**9**)	2096(w), 2070(s), 2051(s), 2032(s), 2019(w), 2009(w), 1992(vw), 1968(vw)	−17.93 [t, 1 H, H^-, ^2J(H–H) = 3.0 Hz] –16.94 [d, 2 H, H^-, ^2J(H–H) = 3.0 Hz] 7.36–7.48 (m, 15 H, $AsPh_3$)	–[d]
$H_3Ru_3Ir(CO)_{11}(SbPh_3)$ (**10**)	2096(w), 2071(s), 2051(vs), 2032(s), 2020(w), 2010(w), 1993(w), 1968(w)	−18.17 [t, 1 H, H^-, ^2J(H–H) = 3.0 Hz] −17.43 [d, 2 H, H^-, ^2J(H–H) = 3.0 Hz] 7.31–7.64 (m, 15 H, $SbPh_3$)	–[d]

[a] Measured as KBr pastilles (**1**, **3**, **4** and **5**); recorded in THF (**2a** and **2b**); recorded in hexane (**6**, **7a**, **7b**, **8**, **9** and **10**).
[b] Measured in $CDCl_3$ solution at 294 K (**1**, **3–5**, **6** and **9**) and at 213 K (**2a**, **2b**, **7a**, **7b**, **8** and **10**).
[c] Measured in $CDCl_3$ solution at 294 K.
[d] Not recorded.

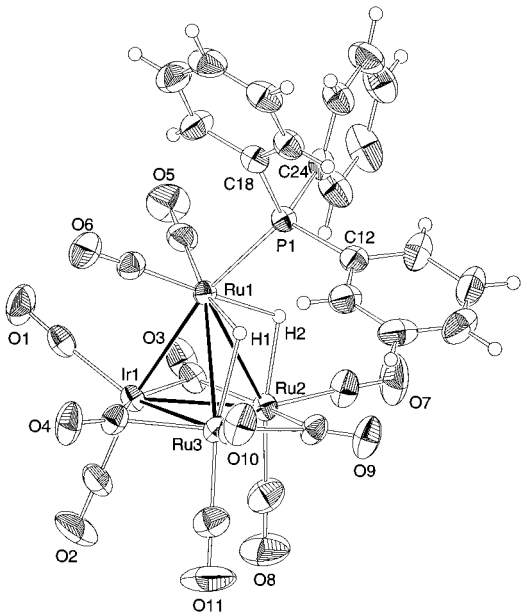

Fig. 1. Molecular structure of cluster anion **1**. ORTEP view (50% probability ellipsoids).

ment of the carbonyls is similar to that in the starting material $[H_2Ru_3Ir(CO)_{12}]^-$, in the Rh homologue $[H_2Ru_3Rh(CO)_{12}]^-$ [15] or other clusters such as $[RuIr_3(CO)_{12}]^-$ [16] and $H_2Ru_2Rh_2(CO)_{12}$ [17]. As observed in the starting compound, and in **1**, a repulsion between the hydride ligands and the nearest equatorial CO groups is found, the bond angles being 115.4(2)° for Ru(1)–Ru(2)–C(7) and 111.7(2)° for Ru(1)–Ru(3)–C(10), whereas the non-bridged edge forms an Ru(1)–Ir(1)–C(1) angle of only 91.4(2)°.

Table 2
Selected bond lengths (Å) and bond angles (°) for anion **1**

Bond length (Å)			
Ir(1)–Ru(1)	2.7549(5)	Ru(1)–H(2)	1.9703(4)
Ir(1)–Ru(2)	2.7403(6)	Ru(2)–H(2)	1.8593(2)
Ir(1)–Ru(3)	2.7642(6)	Ir(1)–C(3)	2.183(6)
Ru(1)–Ru(2)	2.9635(6)	Ru(2)–C(3)	2.059(6)
Ru(1)–Ru(3)	2.9601(6)	Ir(1)–C(4)	2.157(6)
Ru (2)–Ru(3)	2.7791(7)	Ru(3)–C(4)	2.069(5)
Ru(1)–P(1)	2.3410(12)	Ru(2)–C(9)	2.144(6)
Ru(1)–H(1)	1.6250(2)	Ru(3)–C(9)	2.134(5)
Ru(3)–H(1)	1.9885(2)		
Bond angles (°)			
Ru(1)–Ir(1)–Ru(2)	65.27(2)	Ir(1)–Ru(1)–P(1)	168.04(3)
Ru(1)–Ir(1)–Ru(3)	64.87(2)	Ru(2)–Ru(1)–P(1)	112.03(3)
Ru(2)–Ir(1)–Ru(3)	60.64(2)	Ru(3)–Ru(1)–P(1)	113.00(4)
Ir(1)–Ru(1)–Ru(2)	57.13(2)	Ir(1)–C(3)–O(3)	134.3(4)
Ir(1)–Ru(1)–Ru(3)	57.72(2)	Ru(2)–C(3)–O(3)	145.3(5)
Ru(2)–Ru(1)–Ru(3)	55.96(2)	Ir(1)–C(4)–O(4)	136.3(5)
Ir(1)–Ru(2)–Ru(1)	57.60(2)	Ru(3)–C(4)–O(4)	142.0(5)
Ir(1)–Ru(2)–Ru(3)	60.10(2)	Ru(2)–C(9)–O(9)	137.5(4)
Ru(1)–Ru(2)–Ru(3)	61.96(2)	Ru(3)–C(9)–O(9)	141.5(5)
Ir(1)–Ru(3)–Ru(1)	57.41(2)	Ru(1)–Ir(1)–C(1)	91.4(2)
Ir(1)–Ru(3)–Ru(2)	59.25(2)	Ru(1)–Ru(2)–C(7)	115.4(2)
Ru(1)–Ru(3)–Ru(2)	62.08(2)	Ru(1)–Ru(3)–C(10)	111.7(2)

2.3. Synthesis and characterization of the protonated derivatives $H_3Ru_3Ir(CO)_{11}L$ ($L = PPh_3$, PMe_3, $P(OPh)_3$, $AsPh_3$ and $SbPh_3$)

The protonation of the cluster anions $[H_2Ru_3Ir(CO)_{11}L]^-$ (**1**–**5**) with HBF_4 in CH_2Cl_2 leads, within some minutes, to the neutral trihydrido clusters $H_3Ru_3Ir(CO)_{11}(PPh_3)$ (**6**), $H_3Ru_3Ir(CO)_{11}(PMe_3)$ (**7**), $H_3Ru_3Ir(CO)_{11}\{P(OPh)_3\}$ (**8**), $H_3Ru_3Ir(CO)_{11}(AsPh_3)$ (**9**) and $H_3Ru_3Ir(CO)_{11}(SbPh_3)$ (**10**). They were isolated, after thin-layer chromatography, as yellow or orange crystals from a CH_2Cl_2–hexane mixture (Eq. (2)). The PPh_3-substituted cluster **6** is a known compound published recently by Pakkanen and co-workers, who had obtained it by reaction of the anion $[HRu_3(CO)_{11}]^-$ with Vaska's complex $Ir(CO)Cl(PPh_3)_2$ [5]. The trimethylphosphine derivative **7** separates on the thin-layer plates into two isomers, $H_3Ru_3Ir(CO)_{11}(PMe_3)$ (**7a**) and $H_3Ru_3Ir(CO)_{11}(PMe_3)$ (**7b**).

$$[H_2Ru_3Ir(CO)_{11}L]^- + H^+ \longrightarrow H_3Ru_3Ir(CO)_{11}L \quad (2)$$

L	PPh_3	PMe_3	$P(OPh)_3$	$AsPh_3$	$SbPh_3$
	6	**7**	**8**	**9**	**10**

A very similar ν(CO) pattern in the IR spectrum with only terminal absorptions (Table 1) suggests that **6**, **7a**, **8**, **9** and **10** have the same type of structure and the same ligand envelope. The ^{1}H-NMR spectra show, in addition to the signal for the two equivalent hydrides, a second signal for a third hydride ligand as a triplet due to its ^{1}H–^{1}H coupling with the other two hydrides. The resonance of the two equivalent hydrides is observed between δ −16.9 and δ −17.8 ppm, whereas the signal for the third hydride ligand appears between δ −17.4 and δ −18.2 ppm, depending on the ligand L. For compounds $H_3Ru_3Ir(CO)_{11}(PMe_3)$ (**7a**), $H_3Ru_3Ir(CO)_{11}\{P(OPh)_3\}$ (**8**) and $H_3Ru_3Ir(CO)_{11}(SbPh_3)$ (**10**) the signals are temperature-dependent. At room temperature two broad signals (a doublet and a singlet) are observed for the three compounds. By cooling a $CDCl_3$ solution of **7a** down to −60°C, the broad doublet splits into a sharp doublet of doublets (δ −17.80 ppm), and the broad singlet splits into a triplet (δ −18.10 ppm) with a ^2J(H–H) coupling of 3.0 Hz. Similarly, for **8**, the broad doublet also splits at −60°C into a sharp doublet of doublets (δ −17.96 ppm), and the broad singlet splits into a triplet (δ −18.25 ppm) with a ^2J(H–H) coupling of 2.5 Hz. By cooling the $CDCl_3$ solution of **10** down to −60°C, the resonance at δ −17.43 ppm appears as a sharp doublet, and the signal at δ −18.17 ppm splits into a triplet due to the ^2J(H–H) coupling of 3.0 Hz)

Table 3
Selected bond lengths (Å) and bond angles (°) for **8**

Bond length (Å)			
Ir(1)–Ru(1)	2.7474(11)	P(1)–O(13)	1.600(4)
Ir(1)–Ru(2)	2.7474(12)	P(1)–O(14)	1.592(5)
Ir(1)–Ru(3)	2.7466(9)	Ru(1)–H(1)	1.88(9)
Ru(1)–Ru(2)	2.9207(13)	Ru(2)–H(1)	1.88(9)
Ru(1)–Ru(3)	2.9207(15)	Ru(2)–H(2)	1.69(9)
Ru(2)–Ru(3)	2.9405(14)	Ru(3)–H(2)	1.86(9)
Ru(1)–P(1)	2.2642(18)	Ru(1)–H(3)	1.59(10)
P(1)–O(12)	1.598(5)	Ru(3)–H(3)	1.77(11)
Bond angles (°)			
Ru(1)–Ir(1)–Ru(2)	64.22(3)	Ru(1)–Ru(3)–Ru(2)	59.78(3)
Ru(1)–Ir(1)–Ru(3)	64.23(3)	Ir(1)–Ru(1)–P(1)	166.99(4)
Ru(2)–Ir(1)–Ru(3)	64.72(3)	Ru(2)–Ru(1)–P(1)	110.58(5)
Ir(1)–Ru(1)–Ru(2)	57.89(3)	Ru(3)–Ru(1)–P(1)	112.35(5)
Ir(1)–Ru(1)–Ru(3)	57.87(3)	Ru(1)–P(1)–O(12)	121.0(2)
Ru(2)–Ru(1)–Ru(3)	60.45(3)	Ru(1)–P(1)–O(13)	119.5(2)
Ir(1)–Ru(2)–Ru(1)	57.89(3)	Ru(1)–P(1)–O(14)	111.2(2)
Ir(1)–Ru(2)–Ru(3)	57.63(3)	P(1)–O(12)–C(12)	125.1(4)
Ru(1)–Ru(2)–Ru(3)	59.77(3)	P(1)–O(13)–C(18)	126.4(4)
Ir(1)–Ru(3)–Ru(1)	57.90(3)	P(1)–O(14)–C(24)	129.8(4)
Ir(1)–Ru(3)–Ru(2)	57.66(3)		

Table 4
Selected bond lengths (Å) and bond angles (°) for **9**

Bond length (Å)			
Ir(1)–Ru(1)	2.7327(9)	Ru(3)–H(1)	1.80(6)
Ir(1)–Ru(2)	2.7528(12)	Ru(1)–H(2)	1.78(6)
Ir(1)–Ru(3)	2.7354(12)	Ru(2)–H(2)	1.82(6)
Ru(1)–Ru(2)	2.9279(13)	Ru(1)–H(3)	1.80(7)
Ru(1)–Ru(3)	2.9656(11)	Ru(3)–H(3)	1.60(7)
Ru(2)–Ru(3)	2.9236(12)	As(1)–C(12)	1.940(6)
Ru(1)–As(1)	2.4583(11)	As(1)–C(18)	1.934(6)
Ru(2)–H(1)	1.68(6)	As(1)–C(24)	1.935(6)
Bond angles (°)			
Ru(1)–Ir(1)–Ru(2)	64.52(3)	Ir(1)–Ru(3)–Ru(1)	57.11(3)
Ru(1)–Ir(1)–Ru(3)	65.69(3)	Ir(1)–Ru(3)–Ru(2)	58.10(3)
Ru(3)–Ir(1)–Ru(2)	64.38(3)	Ru(2)–Ru(3)–Ru(1)	59.62(3)
Ir(1)–Ru(1)–Ru(2)	58.08(3)	Ir(1)–Ru(1)–As(1)	163.53(3)
Ir(1)–Ru(1)–Ru(3)	57.20(3)	Ru(2)–Ru(1)–As(1)	116.38(4)
Ru(2)–Ru(1)–Ru(3)	59.48(3)	Ru(3)–Ru(1)–As(1)	106.35(3)
Ir(1)–Ru(2)–Ru(1)	57.41(3)	Ru(1)–As(1)–C(12)	113.14(18)
Ir(1)–Ru(2)–Ru(3)	57.52(3)	Ru(1)–As(1)–C(18)	120.09(18)
Ru(3)–Ru(2)–Ru(1)	60.90(3)	Ru(1)–As(1)–C(24)	114.28(17)

(Table 1). The ^{31}P-NMR spectra for **6**, **7a** and **8** exhibit in each case one signal: a multiplet at δ 34.19 ppm (for **6**), a multiplet at δ −4.20 ppm (for **7a**) and a triplet at δ 122.92 ppm (for **8**) with a ^2J(P–H) coupling constant of 10.5 Hz.

The neutral complex $H_3Ru_3Ir(CO)_{11}(PMe_3)$ (**7b**), which crystallizes as red pyramids from a saturated CH_2Cl_2–hexane solution, after chromatographic separation from the isomer **7a** shows almost the same ν(CO) pattern as **7a**, indicating the presence of only terminal carbonyl ligands. The ^{1}H-NMR spectrum of **7b** exhibits only one doublet signal at δ −17.79 ppm with a coupling constant of 5.9 Hz at room temperature (at −60°C: 10.8 Hz). Upon cooling of the $CDCl_3$ solution down to −60°C, three additional hydride signals appear (δ −16.75, δ −20.13, δ −20.17 ppm), which are assigned the third hydride ligand being frozen out as a μ_2-bridge over three different Ru–Ru bonds [Ru(1)–Ru(2), Ru(1)–Ru(3), Ru(2)–Ru(3)]. A similar fluxionality of the hydride ligands (five signals at −80°C) has been observed by Pakkanen and coworkers for the isostructural cluster $H_3Ru_3Ir(CO)_{11}$-(PPh_3) [5]. In the ^{31}P-NMR spectrum a multiplet signal is observed at δ −4.20 ppm (Table 1).

2.4. Molecular structure of $H_3Ru_3Ir(CO)_{11}\{P(OPh)_3\}$ **8**, $H_3Ru_3Ir(CO)_{11}(AsPh)_3$ **9** and $H_3Ru_3Ir(CO)_{11}(PMe_3)$ **7b**

Suitable crystals of **8**, **9** and **7b** were grown by slow evaporation of saturated solutions in CH_2Cl_2/hexane at room temperature. Selected bond lengths and angles of **8**, **9** and **7b** are collected in Tables 3–5. The ORTEP plots of **8**, **9** and **7b** are illustrated in Figs. 2–4, respectively.

In the structures of **8** and **9**, the Ru_3Ir metal skeleton forms a slightly distorted tetrahedron of three ruthenium atoms (basal triangle) and an apical iridium atom. The ligands $P(OPh)_3$ (in **8**) and $AsPh_3$ (in **9**) are bonded in axial fashion to one of the Ru atoms. For all the Ru–Ir bonds almost the same distance of 2.74 Å (average) is found, whereas the Ru–Ru bonds are significantly longer (average 2.94 Å), caused by one bridging hydride ligand over each Ru–Ru edge. The hydride ligands lie out of the ruthenium plane, on the same side as the phosphine or arsine ligand. All carbonyl groups

Table 5
Selected bond lengths (Å) and bond angles (°) for **7b**

Bond length (Å)			
Ir–Ru(1)	2.9349(10)	Ru(1)–H(1)	1.7733(1)
Ir–Ru(2)	2.9052(10)	Ir–H(2)	1.8056(1)
Ir–Ru(3)	2.8009(9)	Ru(2)–H(2)	1.8081(1)
Ru(1)–Ru(2)	2.7629(13)	Ru(1)–H(3)	1.4861(1)
Ru(1)–Ru(3)	2.8936(12)	Ru(2)–H(3)	1.8139(1)
Ru(2)–Ru(3)	2.7578(13)	P(1)–C(12)	1.800(14)
Ir–P(1)	2.355(3)	P(1)–C(13)	1.840(15)
Ir–H(1)	1.8246(1)	P(1)–C(14)	1.807(16)
Bond angles (°)			
Ru(1)–Ir–Ru(2)	56.47(3)	Ir–Ru(3)–Ru(1)	62.02(3)
Ru(1)–Ir–Ru(3)	60.54(3)	Ir–Ru(3)–Ru(2)	63.01(3)
Ru(2)–Ir–Ru(3)	57.77(3)	Ru(1)–Ru(3)–Ru(2)	58.48(3)
Ir–Ru(1)–Ru(2)	61.22(3)	Ru(1)–Ir–P(1)	114.28(8)
Ir–Ru(1)–Ru(3)	57.44(3)	Ru(2)–Ir–P(1)	117.13(8)
Ru(2)–Ru(1)–Ru(3)	58.30(3)	Ru(3)–Ir–P(1)	173.91(8)
Ir–Ru(2)–Ru(1)	62.31(3)	Ir–P(1)–C(12)	113.9(5)
Ir–Ru(2)–Ru(3)	59.22(3)	Ir–P(1)–C(13)	113.4(4)
Ru(1)–Ru(2)–Ru(3)	63.22(3)	Ir–P(1)–C(14)	115.1(6)

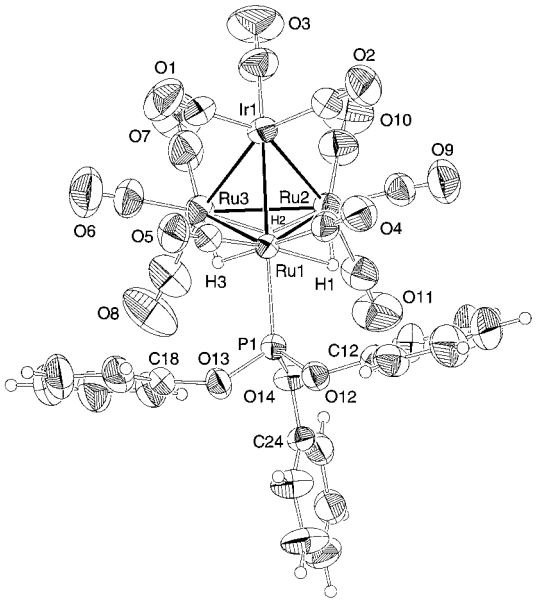

Fig. 2. Molecular structure of **8**. ORTEP view (50% probability ellipsoids).

are terminally coordinated, the Ru carrying the phosphine or arsine ligand is bonded to two CO groups, each of the other ruthenium atoms as well as the apical iridium atom carry three CO ligands.

These structural arrangements are well in line with those found for the PPh_3-homologue $H_3Ru_3Rh(CO)_{11}(PPh_3)$ [5] as well as with those reported for the non-substituted tetranuclear mixed-metal clusters $H_3Ru_3Ir(CO)_{12}$ [18] and $H_3Ru_3Rh(CO)_{12}$ [19] or the osmium homologues $H_3Os_3Ir(CO)_{12}$, $H_3Os_3Rh(CO)_{12}$ [20].

In contrast, the structure of **7b** shows a slightly

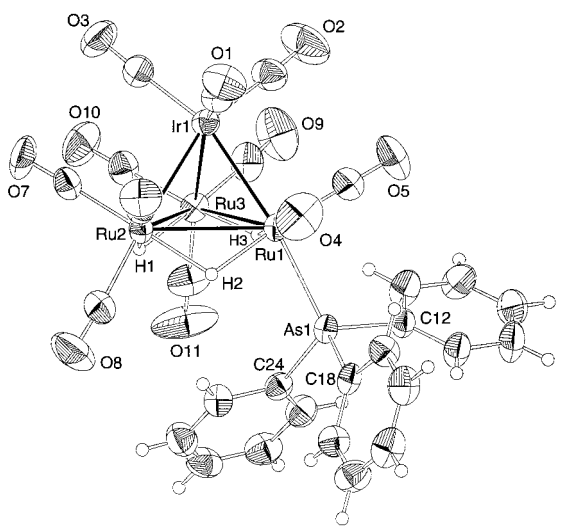

Fig. 3. Molecular structure of **9**. ORTEP view (50% probability ellipsoids).

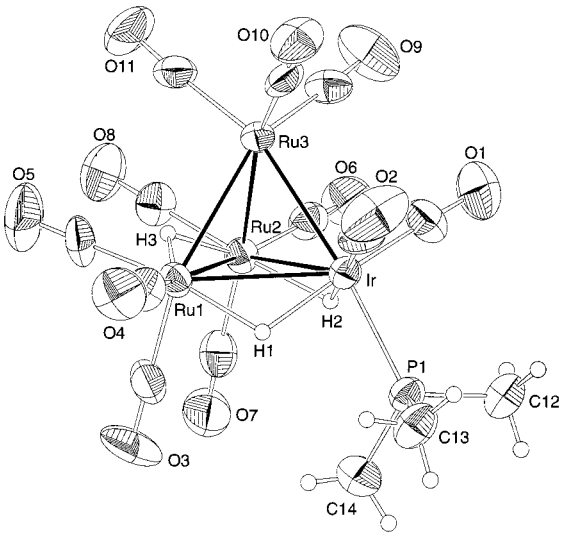

Fig. 4. Molecular structure of **7b**. ORTEP view (50% probability ellipsoids).

different ligand arrangement. The metal framework is also tetrahedral, but more distorted than in **8** or **9**. Two of the ruthenium atoms and the iridium atom form the basal triangle. The PMe_3 ligand is coordinated in an axial fashion to the iridium atom. The iridium atom also carries two terminal carbonyl ligands, while the other nine carbonyls are coordinated to the three ruthenium atoms, each carrying three terminal CO groups. Two of the three hydrido ligands are found to bridge two of the three Ir–Ru bonds, which is also reflected in the longer metal–metal distances: 2.935(1) Å [Ir–Ru(1)] and 2.905(1) Å [Ir–Ru(2)] with respect to 2.801(1) Å for the non-bridged Ir–Ru(3) bond. The third hydrido ligand was difficult to find, however, when compared to the known triphenylphosphine derivative $H_3Ru_3Ir(CO)_{11}(PPh_3)$ [5] it appears to sit over the Ru(1)–Ru(2) edge, despite a relatively short ruthenium–ruthenium distance [2.736(1) Å] as compared to Ru(1)–Ru(3) [2.894(1) Å] and Ru(2)–Ru(3) [2.758(1) Å]. Contrary to H(1) and H(2) which lie below of the Ru_2Ir triangle and in contrast to $H_3Ru_3Ir(CO)_{11}(PPh_3)$ [5], the H(3) bridge is bent upwards, presumably due to an attraction by the electron-deficient ruthenium atom Ru(3), which could also explain the short Ru(1)–Ru(2) distance.

3. Experimental

3.1. General

All reactions were carried out in a nitrogen atmosphere using standard Schlenk techniques. Solvents were distilled over appropriate drying agents [21] and saturated with nitrogen prior to use. Preparative thin-

layer chromatography was performed using 20 × 20 cm plates coated with Fluka Silica Gel G. Infrared spectra were recorded on a Perkin–Elmer 1720X FT-IR spectrometer. The room-temperature NMR spectra were recorded using a Varian Gemini 200 BB instrument, the spectra at −60°C were measured with a Bruker AMX 400 instrument. The spectra were referenced by using the resonance of residual protons in the deuterated solvents. Microanalytical data were obtained from the Mikroelementaranalytisches Laboratorium of the ETH Zürich, Switzerland. The starting compound $[N(PPh_3)_2][H_2Ru_3Ir(CO)_{12}]$ was synthesized according to the published method [3]. The ligands PPh_3, PMe_3, $P(OPh)_3$, $AsPh_3$ (Fluka) and $SbPh_3$ (Aldrich) were purchased and used as received.

3.2. Preparation of the anionic derivatives $[H_2Ru_3Ir(CO)_{11}L]^-$ ($L = PPh_3$ **1**, $P(OPh)_3$ **3**, $AsPh_3$ **4** or $SbPh_3$ **5**)

A THF solution (30 ml) of $[N(PPh_3)_2][H_2Ru_3Ir(CO)_{12}]$ (100 mg, 0.073 mmol) and equimolar amount of the corresponding ligand were placed in a pressure Schlenk tube and heated under stirring for 4 h to 90°C (for $L = PPh_3$, $AsPh_3$ or $SbPh_3$) or 100°C [for $L = P(OPh)_3$]. After removal of the solvent, the products were dissolved in CH_2Cl_2/ether (for $L = PPh_3$) or ethanol (for $L = P(OPh)_3$, $AsPh_3$, $SbPh_3$) and isolated by crystallization from CH_2Cl_2/ether/hexane (20°C) or ethanol/pentane (−20°C), respectively. All compounds were dried in vacuo. $[N(PPh_3)_2]$**1**: yield 92 mg, 78%. Anal. Calc. for $C_{65}H_{47}IrNO_{11}P_3Ru_3 \cdot CH_2Cl_2$: C, 46.86; H, 2.92; N, 0.82. Found: C, 46.80; H, 2.98; N, 0.89. $[N(PPh_3)_2]$**3**: yield 114 mg, 75%. Anal. Calc. for $C_{65}H_{47}IrNO_{14}P_3Ru_3 \cdot 0.7\ C_5H_{12}$: C, 48.25; H, 3.28; N, 0.82. Found: C, 48.32; H, 3.27; N, 0.91. $[N(PPh_3)_2]$**4**: yield 98 mg, 81%. Anal. Calc. for $C_{65}H_{47}AsIrNO_{11}P_2Ru_3 \cdot C_5H_{12}$: C, 48.80; H, 3.45; N, 0.81. Found: C, 48.64; H, 3.50; N, 0.76. $[N(PPh_3)_2]$**5**: yield 92 mg, 74%. Anal. Calc. for $C_{65}H_{47}IrNO_{11}P_2RuSb \cdot 0.6\ C_5H_{12}$: C, 46.92; H, 3.14; N, 0.80. Found: C, 46.90; H, 3.13; N, 0.85.

3.3. Reaction of $[N(PPh_3)_2][H_2Ru_3Ir(CO)_{12}]$ with PMe_3

A THF solution (30 ml) of $[N(PPh_3)_2][H_2Ru_3Ir(CO)_{12}]$ (100 mg, 0.073 mmol), placed in a pressure Schlenk tube, was treated with an excess of a PMe_3 (1 M solution in toluene, 100 μl). The mixture was heated for 4 h at 90°C during which the color changed from orange to yellow. After evaporation of the solvent, the residue was washed twice with 5 ml of hexane and dried in vacuo. The residue was studied by IR, ^{1}H-NMR and ^{31}P-NMR spectroscopy.

3.4. Preparation of the neutral derivatives $H_3Ru_3Ir(CO)_{11}L$ ($L = PPh_3$ **6**, $P(OPh)_3$ **8**, $AsPh_3$ **9** or $SbPh_3$ **10**)

To 20 ml of a CH_2Cl_2 solution of the $[N(PPh_3)_2]^+$ salts of **1** (50 mg, 0.0311 mmol), **3** (80 mg, 0.0383 mmol), **4** (80 mg, 0.0719 mmol) or **5** (80 mg, 0.0690 mmol) an excess of $HBF_4 \cdot OEt_2$ (50 μl) was added. After 15 min of stirring at room temperature the solution was concentrated to a volume of 2 ml. The resulting solutions were submitted to thin-layer chromatography using a mixture of CH_2Cl_2 and hexane (1:2 for **6**, **8** and **9**, 2:3 for **10**) as elutent. The yellow bands containing the products were extracted with CH_2Cl_2, followed by evaporation to dryness. All four compounds were crystallized from CH_2Cl_2/hexane and obtained as yellow or orange crystals. **6**: yield 28 mg, 84%. **8**: yield 32 mg, 74%. Anal. Calc. for $C_{29}H_{18}IrO_{14}PRu_3 \cdot 0.6CH_2Cl_2$: C, 30.44; H, 1.66. Found: C, 30.93; H, 1.63. **9**: yield 48 mg, 88%. Anal. Calc. for $C_{29}H_{18}AsIrO_{11}Ru_3$: C, 31.30; H, 1.63. Found: C, 31.22; H, 1.70. **10**: yield 48 mg, 88%. Anal. Calc. for $C_{29}H_{18}IrO_{11}Ru_3Sb$: C, 30.04; H, 1.56. Found: C, 30.17; H, 1.61.

3.5. Preparation of $H_3Ru_3Ir(CO)_{11}(PMe_3)$ (**7a** and **7b**)

The mixture of **2a** and **2b** (obtained by the reaction of $[H_2Ru_3Ir(CO)_{12}]^-$ with PMe_3 according to Section 3.3) was dissolved in 20 ml of CH_2Cl_2 and protonated by addition of an excess of $HBF_4 \cdot OEt_2$ (40 μl). After 15 min of stirring, the solution was concentrated to a volume of 2 ml and submitted to thin-layer chromatography, using a mixture of CH_2Cl_2 and hexane (1:4) as elutent. The first yellow band, containing **7a** as well as the second orange band, containing **7b** were extracted with CH_2Cl_2. After removal of the solvent the products were crystallized from a CH_2Cl_2/hexane mixture as yellow (**7a**) and red (**7b**) crystals, respectively. Compound **7a**: yield 11 mg 17%. Anal. Calc. for $C_{14}H_{12}IrO_{11}PRu_3 \cdot CH_3OH$: C, 19.69; H, 1.76. Found: C, 19.77; H, 1.65. **7b**: yield 31 mg 48%. Anal. Calc. for $C_{14}H_{12}IrO_{11}PRu_3$: C, 19.05; H, 1.37. Found: C, 19.05; H, 1.41.

3.6. Crystallography

Single crystals were obtained by slow evaporation of saturated solutions in CH_2Cl_2/hexane: yellow blocks for the $[N(PPh_3)_2]^+$ salts of **1**, orange blocks for **8** and **9** and red pyramids for **7b**. Selected crystallographic data for all compounds are summarized in Table 6.

The data for $[N(PPh_3)_2]$**1** were collected at 223 K on a Stoe Imaging Plate Diffractometer System equipped with a one-circle φ goniometer using Mo–K_α graphite-monochromated radiation ($\lambda = 0.71073$ Å, oscillation scans), those for compounds **7b**, **8** and **9** on a Stoe-

Table 6
Crystallographic data for **1**, **7b**, **8** and **9**

Compound	**1**	**7b**	**8**	**9**
Empirical formula	$C_{65}H_{47}IrNO_{11}P_3Ru_3 \cdot CH_2Cl_2$	$C_{14}H_{12}IrO_{11}PRu_3$	$C_{29}H_{18}IrO_{14}PRu_3$	$C_{29}H_{18}AsIrO_{11}Ru_3$
M (g mol^{-1})	1691.28	882.62	1116.81	1112.76
Temperature (K)	223(2)	293(2)	293(2)	293(2)
Crystal system	Triclinic	Monoclinic	Triclinic	Triclinic
Space group	$P\bar{1}$	$P2_1$	$P\bar{1}$	$P\bar{1}$
a (Å)	11.4993(11)	8.2039(6)	10.317(4)	9.356(3)
b (Å)	11.9977(12)	16.3686(9)	10.936(2)	12.062(4)
c (Å)	13.4472(14)	8.6575(5)	15.924(7)	14.956(4)
α (°)	70.267(12)	90	82.88(3)	99.99(3)
β (°)	70.502(11)	98.746(6)	78.47(3)	94.05(3)
γ (°)	80.084(12)	90	81.40(3)	90.67(4)
U (Å^3)	1691.4(3)	1149.07(12)	1732.4(11)	1657.5(9)
Z	1	2	2	2
$D_{calc.}$ (cm^3)	1.710	2.551	2.141	2.230
Crystal dimensions (mm)	$0.6 \times 0.5 \times 0.4$	$0.5 \times 0.5 \times 0.5$	$0.9 \times 0.7 \times 0.45$	$0.8 \times 0.53 \times 0.53$
Color	Yellow	Red	Orange	Orange
μ (mm^{-1})	2.909	7.825	5.222	6.388
F(000)	828	816	1056	1044
θ limits (°)	2.07–25.81	2.38–25.47	2.03–25.47	2.01–25.47
hkl ranges	−14 to 14, −14 to 14, −16 to 16	−9 to 9, 0 to 19, 1 to 10	−12 to 12, −13 to 13, 0 to 19	−11 to 11, −14 to 14, 0 to 18
Transmission factors: min, max	0.266, 0.718	0.0365, 0.0656	0.0462, 0.1144	0.0418, 0.0935
Reflections collected	12809	2210	6428	6133
Independent reflections	10611	2210	6428	6133
Reflections observed $[I = 2\sigma(I)]$	10149	2162	6003	5858
Goodness of fit on F^2 [a]	1.010	1.158	1.285	1.213
Final R indices $[I = 2\sigma(I)]$[b]	$R_1 = 0.0255$, $wR_2 = 0.0619$	$R_1 = 0.0296$, $wR_2 = 0.0772$	$R_1 = 0.0357$, $wR_2 = 0.0976$	$R_1 = 0.0312$, $wR_2 = 0.0837$
R indices (all data)	$R_1 = 0.0270$, $wR_2 = 0.0623$	$R_1 = 0.0306$, $wR_2 = 0.0780$	$R_1 = 0.0423$, $wR_2 = 0.1125$	$R_1 = 0.0344$, $wR_2 = 0.0910$

[a] $S = [\Sigma w(F_o^2 - F_c^2)^2/(n-p)]^{1/2}$ (n number of reflections, p number of parameters).
[b] $R_1 = \Sigma \| F_o | - | F_c \| / \Sigma | F_o |$. $wR_2 = [\Sigma w(F_o^2 - F_c^2)^2 / \Sigma w(F_o)^4]^{1/2}$.

Siemens AED2 4-circle diffractometer at room temperature using also Mo–K_α graphite-monochromated radiation ($\lambda = 0.71073$ Å, ω–2θ scans). The structures of $[N(PPh_3)_2]$**1**, **7b** and **9** were solved by direct methods using the program SHELXS-97 [22], the structure of **8** was solved by Patterson methods also using the SHELXS-97 program. The structure refinement, using weighted full-matrix least-squares on F^2, was carried out using the program SHELXL-97 [23]. For $[N(PPh_3)_2]$**1** an empirical absorption correction was applied using DIFABS [24]. An empirical absorption correction was also applied for compounds **7b**, **8** and **9** using psi scans. Compound $[N(PPh_3)_2]$**1** crystallizes with one disordered molecule of CH_2Cl_2 per asymmetric unit, the two hydrogen atoms were placed in calculated positions and treated as riding atoms using the SHELXL-97 default parameters. All hydride atoms in **1**, **8** and **9** and two of the hydrides in **7b** were located from a difference map and refined isotropically. The third hydride in **7b** was located from difference maps, fixed in the found position and refined isotropically. The methyl and phenyl hydrogen atoms in $[N(PPh_3)_2]$**1**, **7b**, **8** and **9** were included in calculated positions and treated as riding atoms using the SHELXL-97 default parameters. The figures were drawn with ZORTEP [25] (thermal ellipsoids, 50% probability level).

4. Supplementary material

Full tables of atomic parameters, bond lengths and angles are deposited at the Cambridge Crystallographic Data Center, 12 Union Road, Cambridge CB2 1EZ (UK).

Acknowledgements

The authors are grateful to the BASF Aktiengesellschaft for financial support of this work. A generous loan of ruthenium trichloride hydrate by

Johnson Matthey Technology Center is gratefully acknowledged.

References

[1] P. Braunstein, J. Rose, in: E.W. Ebel, F.G.A. Stone, G. Wilkinson (Eds.), Comprehensive Organometallic Chemistry 2, vol. 10, Elsevier, Oxford, 1995, p. 351.
[2] E. Rosenberg, R.M. Laine, in: R.D. Adams, F.A. Cotton (Eds.), Catalysis by Di- and Polynuclear Metal Cluster Complexes, Wiley–VCH, New York, 1998, p. 1.
[3] G. Süss-Fink, S. Haak, V. Ferrand, H. Stoeckli-Evans, J. Chem. Soc. Dalton Trans. (1997) 3861.
[4] G. Süss-Fink, S. Haak, V. Ferrand, H. Stoeckli-Evans, J. Mol. Catal., submitted.
[5] A.U. Härkönen, M. Ahlgrèn, T.A. Pakkanen, J. Pursiainen, Organometallics 16 (1997) 689.
[6] A.U. Härkönen, M. Ahlgrèn, T.A. Pakkanen, J. Pursiainen, J. Organomet. Chem. 530 (1997) 191.
[7] M.J. Mays, P.R. Raithby, P.L. Taylor, K. Henrick, J. Chem. Soc. Dalton Trans. (1984) 959.
[8] H.J. Kakkonen, L. Tunkkari, M. Ahlgrèn, J. Pursiainen, T.A. Pakkanen, J. Organomet. Chem. 496 (1995) 93.
[9] J. Pursiainen, T.A. Pakkanen, J. Jääskeläinen, J. Organomet. Chem. 285 (1985) 85.
[10] H. Matsuzaka, T. Kodama, Y. Uchida, M. Hidai, Organometallics 7 (1988) 1608.
[11] J. Pursiainen, M. Ahlgrèn, T.A. Pakkanen, J. Valkonen, J. Chem. Soc. Dalton Trans. (1990) 1147.
[12] A. Fumagelli, M. Bianchi, M.C. Malatesta, G. Ciani, M. Moret, A. Sironi, Inorg. Chem. 37 (1998) 1324.
[13] H. Kakkonen, M. Ahlgrèn, J. Pursiainen, T.A. Pakkanen, J. Organomet. Chem. 491 (1995) 195.
[14] J. Evans, P.M. Stroud, M. Webster, J. Chem. Soc. Dalton Trans. (1991) 2027.
[15] H.J. Kakkonen, M. Ahlgrèn, T.A. Pakkanen, J. Pursiainen, J. Organomet. Chem. 482 (1994) 279.
[16] A. Fumagelli, F. Demartin, A Sironi, J. Organomet. Chem. 279 (1985) C33.
[17] J. Pursiainen, T.A. Pakkanen, B.T. Heaton, C. Seregni, R.G. Goodfellow, J. Chem. Soc. Dalton Trans. (1986) 681.
[18] Unpublished result.
[19] J. Pursiainen, T.A. Pakkanen, J. Chem. Soc. Dalton Trans. (1989) 2449.
[20] P. Sundberg, B. Norén, B.F.G. Johnson, J. Lewis, P.R. Raithby, J. Organomet. Chem. 353 (1988) 383.
[21] D.D. Perrin, W.L.F. Armarego, Purification of Laboratory Chemicals, Pergamon Press, Oxford, 3rd ed., (1988).
[22] G.M. Sheldrick, Acta Crystallogr. A46 (1990) 647.
[23] G.M. Sheldrick, SHELXL-97, University of Göttingen (1997).
[24] N. Walker, D. Stuart, Acta Crystallogr. A46 (1990) 158.
[25] C.K. Johnson, ZORTEP, Oak Ridge National Laboratory, Oak Ridge, TN, modified for PC by L. Zsolnai, H. Pritzkow, University of Heidelberg (1994).